Multiharmonic Forced Response Analysis of a Turbine Blading Coupled by Nonlinear Contact Forces

Christian Siewert[1]
e-mail: siewert@ids.uni-hannover.de

Lars Panning
e-mail: panning@ids.uni-hannover.de

Jörg Wallaschek
e-mail: wallaschek@ids.uni-hannover.de

Institute of Dynamics and Vibration Research,
Leibniz Universität Hannover,
Appelstraße 11,
30171 Hannover, Germany

Christoph Richter
Steam Turbine Engineering,
Siemens AG-Energy Sector,
Rheinstraße 100,
45478 Mülheim an der Ruhr, Germany
e-mail: christoph-hermann.richter@siemens.com

In turbomachinery applications, the rotating turbine blades are subjected to high static and dynamic loads. The static loads are due to centrifugal stresses and thermal strains whereas the dynamic loads are caused by the fluctuating gas forces resulting in high vibration amplitudes, which can lead to high cycle fatigue failures. Hence, one of the main tasks in the design of turbomachinery blading is the reduction in the blade vibration amplitudes to avoid high dynamic stresses. Thus, coupling devices like underplatform dampers and tip shrouds are applied to the blading to reduce the vibration amplitudes and, therefore, the dynamic stresses by introducing nonlinear contact forces to the system. In order to predict the resulting vibration amplitudes, a reduced order model of a shrouded turbine blading is presented including a contact model to determine the nonlinear contact forces. To compute the forced response, the resulting nonlinear equations of motion are solved in the frequency domain using the multiharmonic balance method because of the high computational efficiency of this approach. The transformation from the time domain into the frequency domain is done by applying Galerkin's method in combination with a multiharmonic approximation function for the unknown vibration response. This results in an algebraic system of nonlinear equations in the frequency domain, which has to be solved iteratively in order to compute the vibration response. The presented methodology is applied to the calculation of the forced response of a nonlinear coupled turbine blading in the frequency domain. [DOI: 10.1115/1.4000266]

1 Introduction

The rotor blades of a low pressure (LP) steam turbine stage are subjected to high static and dynamic loads during operation. The static loads are mainly due to the centrifugal force and thermal strains, whereas the dynamic loads are caused by fluctuating gas forces resulting in forced vibrations of the blades. The forced vibrations can lead to high cycle fatigue (HCF) failures causing substantial damage and high maintenance effort. Thus, one of the main tasks in the design of LP steam turbine blading is the vibration amplitude reduction in order to avoid high dynamic stresses that could damage the blading. The vibration amplitudes of the blades in a LP steam turbine stage can be reduced significantly to a reasonable amount if adjacent blades are coupled by shroud contacts that reinforce the blading, see Fig. 1. Furthermore, in the case of blade vibrations, relative displacements between neighboring blades occur in the contacts and friction forces are generated that provide additional damping to the structure due to the energy dissipation caused by microslip and macroslip effects. Therefore, the coupling of the blades increases the overall mechanical damping. A three-dimensional structural dynamics model including an appropriate spatial contact model is necessary to predict the contact forces generated by the shroud contacts and to describe the vibrational behavior of the blading with sufficient accuracy. To compute the nonlinear forced vibrations of the coupled blading, the nonlinear equations of motion (EQM) are solved in the frequency domain owing to the high computational efficiency of this approach. The transformation of the nonlinear equations of motion into the frequency domain can be carried out by representing the steady-state displacement in terms of its harmonic components. After that transformation, the nonlinear forced response is computed as a function of the excitation frequency in the frequency domain.

One of the first models for the analysis of a turbine blading coupled by shrouds with a higher level of detail was published in Ref. [1]. In this publication, the authors developed useful guidelines for the design of the shroud contact angle. More sophisticated models for the dynamics of a turbine blading coupled by shrouds can be found in Refs. [2,3]. In these publications, the contact model developed by the authors has been extended from a two-dimensional contact model to a full three-dimensional contact model capable to represent the stick, the slip, and the separation contact condition. In Ref. [4], a model for the vibration analysis of the blades coupled by shrouds was presented including a contact model, which is based on a spatial discretization of the contact surface in combination with a quasi three-dimensional contact model. The quasi three-dimensional contact model is also presented in Ref. [5]. This contact model is also applied in Ref. [6] to an underplatform damper with flat contact surfaces (cottage roof damper). The descriptions of actual design concepts for turbine bladings coupled by shroud contacts can be found in Refs. [7,8]. An analysis of the resulting friction damping generated in shroud and snubber contacts of a LP steam turbine blading is given in Ref. [9].

In all the mentioned publications, the classical harmonic balance method that uses only the fundamental harmonic component for the transformation into the frequency domain was applied in order to compute the nonlinear forced response in the frequency domain. However, it was noted in many publications that this single harmonic approximation was often unable to accurately capture the nonlinear forced response, see Poudou and Pierre [10] for example. Therefore, the multiharmonic balance method (MHBM) was developed, which uses a multiharmonic approach

[1]Corresponding author.

Contributed by the International Gas Turbine Institute of ASME for publication in the JOURNAL OF ENGINEERING FOR GAS TURBINES AND POWER. Manuscript received April 14, 2009; final manuscript received September 8, 2009; published online May 26, 2010. Editor: Dilip R. Ballal.

Fig. 1 Low pressure steam turbine blading with a shroud coupling (courtesy of Siemens AG-Energy Sector)

for the transformation of the nonlinear equations of motion into the frequency domain instead of a monofrequent approach. The multiharmonic balance method is able to accurately and efficiently predict the nonlinear forced response of coupled turbine bladings as shown in Refs. [11–13], for example.

In this paper, the multiharmonic balance method is applied to the analysis of a cyclic symmetric shrouded turbine blading in order to compute the nonlinear forced response. Exploiting the cyclic symmetry of the system, it is possible to represent a full bladed disk model by a single cyclic sector model reducing the size of problem. An efficient procedure has been developed that computes the nonlinear contact forces as well as the corresponding tangent stiffness matrix. The proposed multiharmonic balance method for cyclic symmetric systems is exemplified on a finite element model of a shrouded turbine blading.

2 Dynamic Model of a Turbine Blading With Friction Contacts

2.1 EQM of the Turbine Blading. The EQM of a tuned turbine blading with shroud contacts will be derived in this section. In Fig. 2, a schematic diagram of a turbine blading coupled by shrouds is shown. Because the considered blading is assumed to be tuned, the bladed disk is composed of n_s segments with identical mechanical properties, that is, mistuning effects are neglected. This implies that all shroud contacts are assumed to have also identical mechanical properties. This so-called cyclic symmetry of the structure makes it possible to compute the nonlinear dynamics of the shrouded turbine blading just based on a single segment model using appropriate cyclic symmetry constraints, e.g., Refs. [10,12]. The starting point for the derivation the governing EQM of the cyclic segment model is an isolated single segment model subjected to a periodic excitation force and to nonlinear contact forces at the shroud, see Fig. 2. The cyclic segment model of the considered shrouded turbine blading is then obtained from the isolated segment model by imposing proper

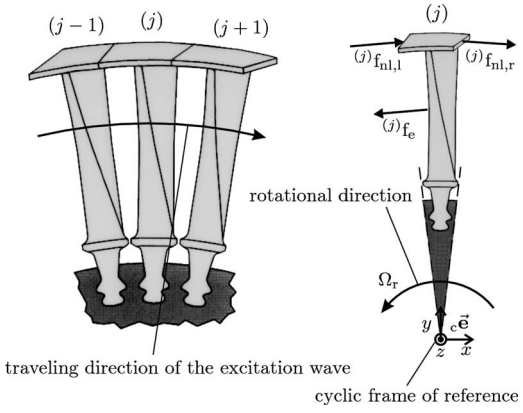

Fig. 2 Cyclic symmetric shrouded blade model

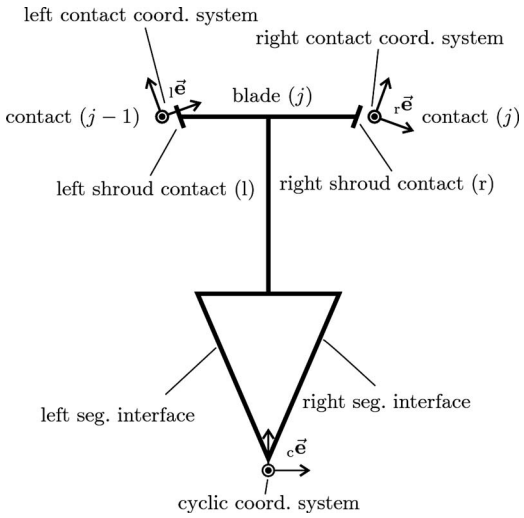

Fig. 3 Schematic view of the segment model with the used coordinate systems

cyclic constraints to the segment's degrees of freedom (DOF) and to the nonlinear contact forces. This approach represents an alternative, that is more suitable to the finite element method (FEM), to the derivation of the EQM based on the full system as presented in Ref. [14].

It is assumed that the turbine blading can be treated as a linear elastic structure. Applying the FEM, the dynamics of the isolated single segment j, $j=1(1)n_s$, can be computed in the time domain by the following nonlinear ordinary differential equation

$$\mathbf{M}_s {}^{(j)}\ddot{u}_s + \mathbf{C}_s {}^{(j)}\dot{u}_s + \mathbf{K}_s {}^{(j)}\mathbf{u}_s = - {}^{(j)}\mathbf{f}_{s,nl} + {}^{(j)}\mathbf{f}_{s,e} \tag{1}$$

This EQM is formulated in a coordinate system that can be viewed as the cyclic frame of reference of the jth segment fixed to the rotor, see Figs. 2 and 3. In Eq. (1), the real and symmetric matrices $\mathbf{M}_s$, $\mathbf{C}_s$, and $\mathbf{K}_s$ denote the mass, the viscous material damping, and the stiffness matrix and the vector ${}^{(j)}\mathbf{u}_s$ the nodal displacements of the considered jth isolated segment model, i.e., a model without cyclic boundary conditions. In the following it is assumed that the viscous material damping matrix $\mathbf{C}_s$ is determined by Rayleigh's damping hypothesis, that is $\mathbf{C}_s = \alpha\mathbf{M}_s + \beta\mathbf{K}_s$ [15]. On the right-hand side of Eq. (1), the vector ${}^{(j)}\mathbf{f}_{s,e}$ represents the excitation forces acting on the airfoil of the jth blade and the vector ${}^{(j)}\mathbf{f}_{s,nl}$ represents the contact forces acting on the left (index l) on the right (index r) shroud contact of the jth blade, see Fig. 2. These contact forces depend nonlinearly on the shroud contact relative displacements.

The EQM are formulated in a rotating, i.e., noninertial, frame of reference fixed to the rotor spinning with the constant angular velocity Ω_r, see Fig. 2. Therefore, the stiffness matrix $\mathbf{K}_s$ generally includes terms accounting for the rotational effects in addition to the elastic stiffness matrix $\mathbf{K}_{s,e}$. These additional terms consist of a geometric stiffness matrix $\mathbf{K}_{s,g}(\Omega_r)$ describing the stiffening effect of the centrifugal forces [15] and a spin-softening matrix $\mathbf{K}_{s,m} = -\Omega_r^2 \mathbf{M}_{s,m}$ describing the stiffness softening due to the changing direction of the centrifugal forces [16]. Thus, the stiffness matrix $\mathbf{K}_s$ used in Eq. (1) reads as follows:

$$\mathbf{K}_s = \mathbf{K}_{s,e} + \mathbf{K}_{s,g}(\Omega_r) - \Omega_r^2 \mathbf{M}_{s,m} \tag{2}$$

Note that the mass matrix $\mathbf{M}_s$ is not identical to the spin-softening mass matrix $\mathbf{M}_{s,m}$, see Gasch and Knothe [16]. It is also possible to include a skew-symmetric gyroscopic matrix $\mathbf{G}_s$ in the EQM in order to consider the Coriolis forces, but in the following these effects are assumed to be negligible.

The displacement vector ${}^{(j)}\mathbf{u}_s$ of the jth isolated segment model used in Eq. (1) can be written as

$$ {}^{(j)}\mathbf{u}_s = \left[{}^{(j)}\mathbf{u}_l^T \quad {}^{(j)}\mathbf{u}_r^T \quad {}^{(j)}\mathbf{u}_m^T \quad {}^{(j)}\mathbf{u}_o^T \right]^T \tag{3} $$

where the vector ${}^{(j)}\mathbf{u}_l$ contains the nodal DOF of the left cyclic segment boundary interface (the interface between the segments $j-1$ and j), the vector ${}^{(j)}\mathbf{u}_r$ contains the nodal DOF of the right cyclic segment boundary interface (the interface between the segments j and $j+1$), the vector ${}^{(j)}\mathbf{u}_m$ contains the nodal master DOF and the vector ${}^{(j)}\mathbf{u}_o$ contains the remaining other nodal DOF. Note that the nodal DOF where the nonlinear contact forces as well as the nodal DOF where the excitation forces act on are a subset of the master DOF, that is $[{}^{(j)}\mathbf{u}_{nl,l}^T \quad {}^{(j)}\mathbf{u}_{nl,r}^T]^T \subset {}^{(j)}\mathbf{u}_m$ and ${}^{(j)}\mathbf{u}_e \subset {}^{(j)}\mathbf{u}_m$. Thus, imposing cyclic symmetry constraints to the DOF located at the left and at the right segment interface, that is ${}^{(j)}\mathbf{u}_l$ and ${}^{(j)}\mathbf{u}_r$, has no *direct* effect on these DOF. The structural matrices of the considered isolated segment are partitioned according to the structure of the displacement vector given in Eq. (3). The structural matrices for the considered isolated segment can be easily computed using commercial finite element codes like ANSYS. The computed matrices can be exported, so they are available for the use in an external nonlinear forced response code.

In the following, it is assumed that the considered turbine blading is subjected to a so-called traveling wave type excitation, see Refs. [10,12,14]. As the bladed disk rotates with the angular velocity Ω_r, it is subjected to the pressure field, which has a constant but nonuniform spatial periodic distribution with respect to a cyclic inertial frame of reference. The integration of this pressure field in the sense of the FEM results in the consistent nodal excitation forces [15]. Because of the spatial periodicity of the pressure field, the resulting consistent nodal forces exhibit also a spatial periodicity in the cyclic inertial frame of reference and can therefore be expanded in terms of an infinite Fourier series. Truncating this infinite Fourier series to n_h harmonics and transformation of the excitation forces into cyclic rotating frame of reference fixed to the rotor results in the periodic excitation of the jth segment, which reads

$$ {}^{(j)}\mathbf{f}_{s,e} = \Re\left\{ \sum_{n=0}^{\infty} {}^{(j)}\hat{\mathbf{f}}_{s,e}^{(n)} e^{in\tau} \right\} = \Re\left\{ \sum_{n=0}^{\infty} {}^{(1)}\hat{\mathbf{f}}_{s,e}^{(n)} e^{in(\tau-(j-1)\delta_m)} \right\} \tag{4} $$

for $j=1(1)n_s$ using the phase shift angle defined as $\delta_m = m\delta$ with the segment angle $\delta = 2\pi/n_s$, the fundamental spatial periodicity m and the dimensionless time τ defined as $\tau = m\Omega_r t$. Note that in the case of a monofrequent traveling wave type excitation, the spatial periodicity m is also called the engine order (EO) and consequently, the traveling wave type excitation is referred to as an engine order excitation. From Eq. (4), it can be seen that the excitation forces formulated in the cyclic rotating frame of reference represent a traveling wave type excitation, which is traveling in the opposite direction to the rotational direction of the rotor, see Fig. 2.

2.2 The MHBM for the Calculation of the Steady-State Solution. The steady-state response of the considered jth segment is of interest when the turbine blading is subjected to a periodic excitation as in the case of the considered traveling wave type excitation. To compute the steady-state response, the nonlinear EQM given in Eq. (1) are solved in the frequency domain owing to the high computational efficiency of this approach. To this end, Galerkin's method is used in combination with truncated Fourier series representation of the displacements and of the nonlinear contact forces to obtain an approximate solution of the steady-state response. The use of Galerkin's method in combination with an approximation of unknown displacements in terms of a truncated Fourier series is also known as the multiharmonic balance method. Therefore, the displacement vector ${}^{(j)}\mathbf{u}_s$ of the jth segment can by written as

$$ {}^{(j)}\mathbf{u}_s = \Re\left\{ \sum_{n=0}^{n_h} {}^{(j)}\hat{\mathbf{u}}_s^{(n)} e^{in\tau} \right\} \tag{5} $$

Furthermore, since the displacements are assumed to be periodic and since the contact forces depend nonlinearly on the relative displacements that are also periodic since they are computed from the periodic displacements, the nonlinear contact forces ${}^{(j)}\mathbf{f}_{s,nl}$ are also expressed in terms of truncated Fourier series and read as

$$ {}^{(j)}\mathbf{f}_{s,nl} = \Re\left\{ \sum_{n=0}^{n_h} {}^{(j)}\hat{\mathbf{f}}_{s,nl}^{(n)} e^{in\tau} \right\} \tag{6} $$

The number of harmonics n_h in Eqs. (5) and (6) must be chosen to approximate the dynamics of the structure with sufficient accuracy. It is assumed that the periodic response of the structure given in Eq. (5) contains only superharmonics of the fundamental period of vibration $T = 2\pi/m\Omega_r$, where m is again the spatial periodicity of the response, but it is easily possible to modify this truncated Fourier series approximation in order to include subharmonics into the analysis. Using the Fourier series expressions for the excitation in Eq. (4), for the displacements in Eq. (5), and for the nonlinear contact forces in Eq. (6) in the complex notation, the EQM given in Eq. (1) for the isolated jth segment can be rewritten as

$$ \sum_{n=0}^{n_h} \left(\left[-(nm\Omega_r)^2 \mathbf{M}_s + inm\Omega_r \mathbf{C}_s + \mathbf{K}_s \right] {}^{(j)}\hat{\mathbf{u}}_s^{(n)} + {}^{(j)}\hat{\mathbf{f}}_{s,nl}^{(n)} - {}^{(j)}\hat{\mathbf{f}}_{s,e}^{(n)} \right) e^{in\tau} \approx 0 \tag{7} $$

Note that in this equation the left-hand side is not exactly zero since the Fourier series expression for the segment's displacement vector given in Eq. (5) is only an approximation of the real displacements. By applying Galerkin's procedure to Eq. (7), the EQM can be transformed into the frequency domain and a set of nonlinear algebraic equations is obtained that has to be solved for the unknown amplitudes of the displacement vector, i.e., ${}^{(j)}\hat{\mathbf{u}}_s^{(n)}$ with $n=0(1)n_h$. For $n=0$, the static equilibrium equation

$$ \mathbf{K}_s {}^{(j)}\hat{\mathbf{u}}_s^{(0)} + {}^{(j)}\hat{\mathbf{f}}_{s,nl}^{(0)} - {}^{(j)}\hat{\mathbf{f}}_{s,e}^{(0)} = 0 \tag{8} $$

is obtained and included in the analysis. Introducing the complex segment dynamic stiffness matrix

$$ \hat{\mathbf{S}}_s^{(n)} = -(nm\Omega_r)^2 \mathbf{M}_s + inm\Omega_r \mathbf{C}_s + \mathbf{K}_s \tag{9} $$

for the harmonic component n, $n=1(1)n_h$, the dynamic equilibrium for the nth harmonic component can be written in a form similar to the static equilibrium given in Eq. (9), i.e.,

$$ \hat{\mathbf{S}}_s^{(n)(j)} \hat{\mathbf{u}}_s^{(n)} + {}^{(j)}\hat{\mathbf{f}}_{s,nl}^{(n)} - {}^{(j)}\hat{\mathbf{f}}_{s,e}^{(n)} = 0 \tag{10} $$

for $n=1(1)n_n$. The system of nonlinear equations formed by Eqs. (8) and (10) has to be solved iteratively for the unknown amplitudes of the displacement vector of the jth segment because of the nonlinear contact forces. Note that this system of nonlinear equations still represents the dynamics of an isolated segment model, that is a model without cyclic symmetry constraints. These boundary conditions will be imposed on the system in the next section.

2.3 Formulation of Cyclic Symmetry Constraints. In the first step, the cyclic symmetry constraints are imposed on the linear part of the equation system given by Eqs. (8) and (10) for the nonlinear dynamics of the isolated jth segment. Since the considered bladed disk is excited by a traveling wave type excitation it is assumed that the steady-state vibration response represents also a traveling wave. Therefore, a unique relationship between the nodal DOF of the left segment interface and the nodal DOF of the right segment interface, see Fig. 3, can be formulated in the cyclic frame of reference. This relation for the periodic response can be formulated in the time domain for the considered jth segment and reads

$$^{(j)}\mathbf{u}_r(\tau) = (\mathbf{I} \otimes \mathbf{A})^{(j)}\mathbf{u}_l(\tau - \delta_m) \tag{11}$$

where $\mathbf{I}$ is an identity matrix of appropriate size and the rotation matrix $\mathbf{A}$ defines the coordinate transformation between the cyclic frames of references of adjacent segments. The symbol $\otimes$ used in Eq. (11) defines the Kronecker product. The relationship given in Eq. (11) is used to impose the cyclic symmetry boundary conditions on the linear elastic structure. In accordance with Eq. (5), the truncated Fourier series representation of the nodal DOF of the right segment interface of the jth segment can be written as

$$^{(j)}\mathbf{u}_r = \Re\left\{\sum_{n=0}^{n_h} {}^{(j)}\hat{\mathbf{u}}_r^{(n)} e^{in\tau}\right\} = \Re\left\{\sum_{n=0}^{n_h} e^{-in\delta_m}(\mathbf{I} \otimes \mathbf{A})^{(j)}\hat{\mathbf{u}}_l^{(n)} e^{in\tau}\right\} \tag{12}$$

using Eq. (11). By considering the partitioning of the segment's displacement vector given in Eq. (3), the cyclic constraints for the nth harmonic component can be stated as

$$^{(j)}\hat{\mathbf{u}}_s^{(n)} = \hat{\mathbf{T}}^{(n)(j)}\hat{\mathbf{u}}^{(n)} \tag{13}$$

with the displacement amplitudes of the cyclic segment model of the jth segment

$$^{(j)}\hat{\mathbf{u}}^{(n)} = \left[{}^{(j)}\hat{\mathbf{u}}_l^{(n)^T} \quad {}^{(j)}\hat{\mathbf{u}}_m^{(n)^T} \quad {}^{(j)}\hat{\mathbf{u}}_o^{(n)^T}\right]^T \tag{14}$$

and the cyclic symmetry constraint matrix for the nth harmonic component

$$\hat{\mathbf{T}}^{(n)} = \begin{bmatrix} \mathbf{I} & 0 & 0 \\ e^{-in\delta_m}(\mathbf{I} \otimes \mathbf{A}) & 0 & 0 \\ 0 & \mathbf{I} & 0 \\ 0 & 0 & \mathbf{I} \end{bmatrix} \tag{15}$$

in a more suitable matrix form. Substitution of the vector $^{(j)}\hat{\mathbf{u}}_s^{(n)}$ in Eqs. (8) and (10) by the cyclic constraint expression given in Eq. (13) for $n=0(1)n_h$ and multiplying these equations with the corresponding complex conjugate transpose of the cyclic symmetry constraint matrix from the left-hand side results in

$$\hat{\mathbf{K}}^{(0)(j)}\hat{\mathbf{u}}^{(0)} + {}^{(j)}\hat{\mathbf{f}}_{nl}^{(0)} - {}^{(j)}\hat{\mathbf{f}}_e^{(0)} = 0 \tag{16}$$

for the static equilibrium equation ($n=0$) and in

$$\hat{\mathbf{S}}^{(n)(j)}\hat{\mathbf{u}}^{(n)} + {}^{(j)}\hat{\mathbf{f}}_l^{(n)} - {}^{(j)}\hat{\mathbf{f}}_e^{(n)} = 0 \tag{17}$$

with

$$\hat{\mathbf{S}}^{(n)} = -(nm\Omega_r)^2\hat{\mathbf{M}}^{(n)} + inm\Omega_r\hat{\mathbf{C}}^{(n)} + \hat{\mathbf{K}}^{(n)} \tag{18}$$

for the dynamic equilibrium equation of the nth harmonic component with $n=1(1)n_h$. The complex mass matrix $\hat{\mathbf{M}}^{(n)}$, the viscous material damping matrix $\hat{\mathbf{C}}^{(n)}$, and the stiffness matrix $\hat{\mathbf{K}}^{(n)}$ are hermitian because of the application of the cyclic symmetry constraints to the considered isolated segment model and have the following form:

$$\hat{\alpha}^{(n)} = \alpha_0 + e^{-in\delta_m}\alpha_1 + e^{in\delta_m}\alpha_1^T \tag{19}$$

for $\alpha = \mathbf{M}, \mathbf{C}, \mathbf{K}$. Thus, these matrices depend on the actual harmonic n and on the phase shift angle δ_m [10,17]. Note that only the DOF of the right segment interface DOF are eliminated by imposing the cyclic symmetry constraints. Thus, the vector of the left contact forces, the vector of the right contact forces and the vector of the excitation forces are not directly affected by this operation.

In the second step, the cyclic boundary conditions are imposed on the nonlinear contact forces. As already mentioned, the nonlinear contact forces depend on the relative displacements between the contacting nodes. Using the cyclic symmetry constraints in an analogous way to Eq. (11), the relative displacements of the left shroud contact (contact $j-1$) can be expressed in the left shroud contact coordinate system, see Fig. 3, as follows:

$$\begin{aligned} ^{(j-1)}\mathbf{w}_{nl}(\tau) &= (\mathbf{I} \otimes \mathbf{A}_l)^{(j)}\mathbf{u}_{nl,l}(\tau) - (\mathbf{I} \otimes \mathbf{A}_r)^{(j-1)}\mathbf{u}_{nl,r}(\tau) \\ &= (\mathbf{I} \otimes \mathbf{A}_l)^{(j)}\mathbf{u}_{nl,l}(\tau) - (\mathbf{I} \otimes \mathbf{A}_r)^{(j)}\mathbf{u}_{nl,r}(\tau + \delta_m) \end{aligned} \tag{20}$$

The rotation matrices $\mathbf{A}_l$ and $\mathbf{A}_r$ used in Eq. (20) define the coordinate transformation from the cyclic coordinate system of the considered segment model into the left and the right shroud contact coordinate system, respectively. These two rotation matrices are related by $\mathbf{A}_l = \mathbf{A}_r\mathbf{A}$. The expression for the relative displacement given in Eq. (20) can also be expressed in terms of a truncated Fourier series by using cyclic constraints in a similar way as in Eq. (12), which reads as

$$\begin{aligned} ^{(j-1)}\mathbf{w}_{nl}(\tau) &= \Re\left\{\sum_{n=0}^{n_h} {}^{(j-1)}\hat{\mathbf{w}}_{nl}^{(n)} e^{in\tau}\right\} \\ &= \Re\left\{\sum_{n=0}^{n_h} ((\mathbf{I} \otimes \mathbf{A}_l)^{(j)}\hat{\mathbf{u}}_{nl,l}^{(n)} - e^{in\delta_m}(\mathbf{I} \otimes \mathbf{A}_r)^{(j)}\hat{\mathbf{u}}_{nl,r}^{(n)}) e^{in\tau}\right\} \end{aligned} \tag{21}$$

Comparing the complex Fourier coefficients in Eq. (21) it becomes obvious how to compute the relative displacement amplitudes $^{(j-1)}\hat{\mathbf{w}}_{nl}^{(n)}$. The nonlinear contact force at the left shroud contact can be computed based on the given relative displacement using an appropriate contact model as shown in Sec. 4. Since the computed relative displacement is periodic, the resulting nonlinear contact force will also be periodic and can be written as

$$^{(j)}\mathbf{f}_{nl,l}(\tau) = \Re\left\{\sum_{n=0}^{n_h} {}^{(j)}\hat{\mathbf{f}}_{nl,l}^{(n)} e^{in\tau}\right\} \tag{22}$$

formulated in the left shroud contact coordinate system. Since the forced response computation is performed in the cyclic coordinate system of the jth segment, the contact forces in Eq. (22) have be transformed from the left shroud contact coordinate system into the cyclic coordinate system using the extended rotation matrix $\mathbf{I} \otimes \mathbf{A}_l^T$. Because of the assumed cyclic symmetry of the considered system and because of Newton's third law, the nonlinear contact forces acting on the right shroud contact of the considered jth segment, that is $^{(j)}\mathbf{f}_{nl,r}(\tau)$, can directly be obtained from $^{(j)}\mathbf{f}_{nl,l}(\tau)$ by

$$^{(j)}\mathbf{f}_{nl,r}(\tau) = -{}^{(j)}\mathbf{f}_{nl,l}(\tau - \delta_m) \tag{23}$$

Note that the right shroud contact forces $^{(j)}\mathbf{f}_{nl,r}(\tau)$ are formulated in the right shroud contact coordinate system. Therefore, a coordinate transformation using the extended rotation matrix $\mathbf{I} \otimes \mathbf{A}_r^T$ is again necessary in order to express the right shroud contact forces in the cyclic coordinate system of the jth segment. Using Eqs. (22) and (23), the right shroud contact forces can be rewritten as

$$^{(j)}\mathbf{f}_{nl,r}(\tau) = \Re\left\{\sum_{n=0}^{n_h} {}^{(j)}\hat{\mathbf{f}}_{nl,r}^{(n)} e^{in\tau}\right\} = -\Re\left\{\sum_{n=0}^{n_h} e^{-in\delta_m(j)}\hat{\mathbf{f}}_{nl,l}^{(n)} e^{in\tau}\right\} \tag{24}$$

With Eq. (22) and Eq. (24) and the proper extended rotation matrices, the only nonzero component of the nonlinear contact force amplitude $^{(j)}\hat{\mathbf{f}}_{nl}$ formulated in the cyclic frame of reference can finally be expressed as

$$\begin{bmatrix} (\mathbf{I} \otimes \mathbf{A}_l^T)^{(j)}\hat{\mathbf{f}}_{nl,l}^{(n)} \\ (\mathbf{I} \otimes \mathbf{A}_r^T)^{(j)}\hat{\mathbf{f}}_{nl,r}^{(n)} \end{bmatrix} = \begin{bmatrix} (\mathbf{I} \otimes \mathbf{A}_l^T)^{(j)}\hat{\mathbf{f}}_{nl,l}^{(n)} \\ -e^{-in\delta_m}(\mathbf{I} \otimes \mathbf{A}_r^T)^{(j)}\hat{\mathbf{f}}_{nl,l}^{(n)} \end{bmatrix} \subset {}^{(j)}\hat{\mathbf{f}}_{nl}^{(n)} \tag{25}$$

for $n=0(1)n_h$.

2.4 Contact Model. The contact forces at a particular contact node pair of the left shroud contact are computed for a given three-dimensional periodic relative displacement using a three-dimensional node-to-node contact element. This element is based

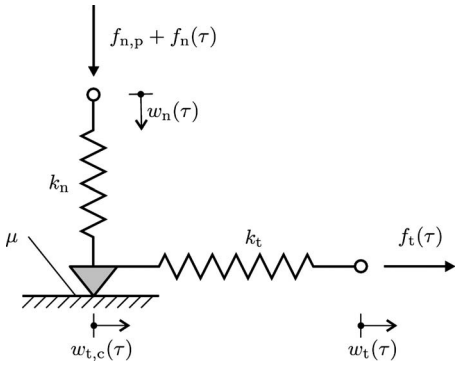

Fig. 4 One-dimensional contact model with normal load variation

on the one-dimensional friction contact model with normal load variation that is widely used in the nonlinear forced response analysis of frictional constraint structures [18,19]. A schematic view of this contact model is shown in Fig. 4. The three-dimensional relative displacement is expressed in the shroud contact coordinate system and decomposed into two perpendicular one-dimensional in-plane tangential components $w_{t,1}(\tau)$ and $w_{t,2}(\tau)$ and an out-of-plane normal component $w_n(\tau)$. The one-dimensional friction contact model with normal load variation is employed because it is assumed that the in-plane tangential components of the contact force are independent from each other. This assumption is commonly used in the calculation of the nonlinear forced response of structures with frictional constraints, see Refs. [19–23]. A fully coupled version of the node-to-node contact element is presented in Refs. [4,5].

The one-dimensional contact model with normal load variation is used to compute the periodic contact forces, i.e., the friction and the unilateral contact force at the interacting contact node pair, for a given periodic relative displacement taking into account a possible separation of the normal contact and the stick-slip-separation contact states of the tangential contact. The tangential friction forces are governed by the Coulomb friction law. The possibility to model an initial gap that affects the normal force as well as the tangential force is also included in the model. The parameters of the one-dimensional friction contact model with normal load variation are the tangential contact stiffness k_t, the normal contact stiffness k_n, the coefficient of friction μ, and the normal preload $f_{n,p}$, see Fig. 4. An initial gap between the nodes of the considered contact node pair can be modeled by $g_{n,p}=-f_{n,p}/k_n$. The resulting nonlinear normal and tangential contact forces can be expressed as follows.

Along the normal direction, an elastic unilateral contact law is defined as

$$f_n(\tau) = \max(f_{n,p} + k_n w_n(\tau), 0) \tag{26}$$

Along the tangential direction, the contact force is defined as

$$f_t(\tau) = \begin{cases} k_n(w_n(\tau) - w_{n,c}) & \text{stick} \\ \mu f_n(\tau)\text{sgn}(w_{n,c}(\tau)) & \text{slip} \\ 0 & \text{separation} \end{cases} \tag{27}$$

Depending on the normal as well as the tangential contact state with the tangential displacement of the Coulomb slider $w_{t,c}(\tau)$, see Fig. 4.

The transition criteria between the individual contact states are detailed in Refs. [18,19]. Using this one-dimensional contact model with normal load variation, the time history of the normal as well as of the tangential contact force can be computed for a given periodic normal and tangential relative displacement. Since the EQM for the steady-state response are formulated in the frequency domain, the Fourier coefficients of the nonlinear contact forces have to be computed for a given set of the Fourier coefficients of the corresponding relative displacement. This is done using the alternating frequency time (AFT) method developed in Ref. [24], also known as the hybrid frequency time (HFT) method [10]. In computational applications, the idea of the AFT/HFT method is to use the fast Fourier transformation (FFT), see Newland [25], to derive the Fourier coefficients of the nonlinear forces that are evaluated in the time domain for given relative displacements, see Fig. 5. This method is very flexible because the nonlinear contact force is computed in the time domain. Thus, a large number of different contact models, including for example microslip and macroslip models, can be easily used within this framework making this method superior to other procedures. The key feature of this approach is the extensive use of the FFT leading to a high computational efficiency.

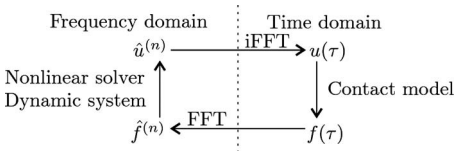

Fig. 5 Diagram of the AFT/HFT method

The relative normal and tangential displacements are computed in the time domain from their Fourier coefficients $\hat{w}_t^{(n)}$ and $\hat{w}_n^{(n)}$, $n=0(1)n_h$, using the inverse FFT. This results in the time history of the relative displacements evaluated at lth discrete time step as

$$w_{n/t}(l) = \sum_{k=0}^{N-1} \hat{w}_{n/t}^{(k)} e^{ikl2\pi/N} \quad \text{for} \quad l = 0(1)N-1 \tag{28}$$

where N is the size of the FFT with $n_h \ll N$. The corresponding contact forces are also determined at the discrete times and can be computed efficiently using a time marching procedure [13]. The normal contact force at the lth time step is computed by

$$f_n(l) = \max(f_{n,p} + k_n w_n(l), 0) \tag{29}$$

The tangential contact forces calculation is based on a predictor-corrector procedure satisfying at each time step Coulomb's friction law and taking possible separation into account. If the contact state at the lth time step is separation ($f_n(l)=0$) than the resulting tangential contact force is, in according to Eq. (27), zero. Otherwise it has to be checked if the contact is in the stick or in the slip state. To this end, a prediction of the tangential contact force at the lth discrete time step is computed by

$$f_t^p(l) = k_t(w_t(l) - w_{t,c}(l-1)) = k_t(w_t(l) - w_t(l-1)) + f_t(l-1) \tag{30}$$

assuming that the contact is in the stick state. Based on this prediction, the actual tangential contact force at the lth time step can be computed in a correction step and reads as

$$f_t(l) = \begin{cases} 0 & \text{for } f_n(l) = 0 \text{(separation)} \\ f_t^p(l) & \text{for } |f_t^p(l)| < \mu f_n(l) \text{(stick)} \\ \mu f_n(l)\text{sgn}(f_t^p(l)) & \text{for } |f_t^p(l)| \geq \mu f_n(l) \text{(slip)} \end{cases} \tag{31}$$

The tangential displacement of the Coulomb slider is updated at the lth time step by

$$w_{t,c}(l) = \begin{cases} w_t(l) & \text{separation} \\ w_{t,c}(l-1) & \text{stick} \\ w_t(l) - \dfrac{f_t(l)}{k_t} & \text{slip} \end{cases} \tag{32}$$

After the periodic time history of the tangential and normal contact forces are evaluated by this time marching procedure, the corresponding Fourier coefficients are computed by the FFT

$$\hat{f}_{n/t}^{(k)} = \frac{1}{N}\sum_{l=0}^{N-1} f_{n/t}(l) e^{-ikl2\pi/N} \quad \text{for } k = 0(1)N-1 \tag{33}$$

Note that only the first n_h harmonic components of the normal and the tangential contact forces are needed for the forced response computation, but the FFT computes the Fourier coefficients up to the $N/2$-th harmonic component [25]. This can be used to check if the chosen number of harmonics n_h is sufficient for the nonlinear analysis [26].

Following the idea of Cardona et al. [27], not only the Fourier coefficients of the nonlinear contact forces but also the corresponding tangent stiffness matrix that is needed for the efficient iterative solution of the EQM can be computed using the AFT/HFT procedure. The partial derivatives $\partial\Re\{\hat{f}_{n/t}^{(k)}\}/\partial\Re\{\hat{w}_{n/t}^{(h)}\}$, $\partial\Re\{\hat{f}_{n/t}^{(k)}\}/\partial\Im\{\hat{w}_{n/t}^{(h)}\}$, $\partial\Im\{\hat{f}_{n/t}^{(k)}\}/\partial\Re\{\hat{w}_{n/t}^{(h)}\}$, and $\partial\Im\{\hat{f}_{n/t}^{(k)}\}/\partial\Im\{\hat{w}_{n/t}^{(h)}\}$ for $k,h=0(1)n_h$ have to be computed in order to build up the tangent stiffness matrix. The AFT/HFT computation of these partial derivatives will be exemplified on the following computation of the partial derivatives of the kth Fourier coefficient of the contact normal force with respect to the real and the imaginary part of the hth Fourier coefficient of the normal relative displacement that reads as

$$\frac{\partial\hat{f}_n^{(k)}}{\partial\Re\{\hat{w}_n^{(h)}\}} = \frac{\partial\Re\{\hat{f}_n^{(k)}\}}{\partial\Re\{\hat{w}_n^{(h)}\}} + i\frac{\partial\Im\{\hat{f}_n^{(k)}\}}{\partial\Re\{\hat{w}_n^{(h)}\}} = \frac{1}{N}\sum_{l=0}^{N-1}\frac{\partial f_n(l)}{\partial\Re\{\hat{w}_n^{(h)}\}} e^{-ikl2\pi/N}$$
$$= \frac{1}{N}\sum_{l=0}^{N-1}\frac{\partial f_n(l)}{\partial w_n}\cos\left(hl\frac{2\pi}{N}\right)e^{-ikl2\pi/N} \tag{34}$$

and

$$\frac{\partial\hat{f}_n^{(k)}}{\partial\Im\{\hat{w}_n^{(h)}\}} = \frac{\partial\Re\{\hat{f}_n^{(k)}\}}{\partial\Im\{\hat{w}_n^{(h)}\}} + i\frac{\partial\Im\{\hat{f}_n^{(k)}\}}{\partial\Im\{\hat{w}_n^{(h)}\}} = \frac{1}{N}\sum_{l=0}^{N-1}\frac{\partial f_n(l)}{\partial\Im\{\hat{w}_n^{(h)}\}} e^{-ikl2\pi/N}$$
$$= \frac{1}{N}\sum_{l=0}^{N-1} -\frac{\partial f_n(l)}{\partial w_n}\sin\left(hl\frac{2\pi}{N}\right)e^{-ikl2\pi/N} \tag{35}$$

Therefore, the AFT/HFT computation of the nonlinear contact forces Fourier coefficient's partial derivatives with respect to the Fourier coefficients of the relative displacements can be performed by evaluating the FFT of the corresponding derivative formulated in the time domain multiplied by sine and cosine functions. The partial derivatives in the time domain are easy to evaluate as soon as the corresponding contact state is known. The derivative of the normal contact force with respect to a real part of the hth Fourier coefficient of the normal relative displacement is given by

$$\frac{\partial f_n(l)}{\partial\Re\{\hat{w}_n^{(h)}\}} = \begin{cases} 0 & \text{separation} \\ k_n\cos\left(hl\dfrac{2\pi}{N}\right) & \text{contact} \end{cases} \tag{36}$$

The derivatives of the normal contact force with respect to the imaginary parts of the normal relative displacements are computed in a similar way. The derivatives of the normal contact force with respect to all Fourier coefficients of the tangential relative displacement are zero. The derivative of the tangential contact force with respect to the real part of the hth Fourier coefficient of the tangential relative displacement reads as

$$\frac{\partial f_t(l)}{\partial\Re\{\partial\hat{w}_t^{(h)}\}} = \begin{cases} 0 & \text{separation} \\ k_t\left(\cos\left(hl\dfrac{2\pi}{N}\right) - \cos\left(h(l-1)\dfrac{2\pi}{N}\right)\right) + \dfrac{\partial f_t(l-1)}{\partial\Re\{\partial\hat{w}_t^{(h)}\}} & \text{stick} \\ 0 & \text{slip} \end{cases} \tag{37}$$

and the derivative of the tangential contact force with respect to the real part of the hth Fourier coefficient of the normal relative displacement

$$\frac{\partial f_t(l)}{\partial\Re\{\partial\hat{w}_n^{(h)}\}} = \begin{cases} 0 & \text{separation} \\ \dfrac{\partial f_t(l-1)}{\partial\Re\{\partial\hat{w}_n^{(h)}\}} & \text{stick} \\ \mu k_n\cos\left(hl\dfrac{2\pi}{N}\right)\operatorname{sgn}(f_t^p(l)) & \text{slip} \end{cases} \tag{38}$$

Again, the derivatives with respect to the imaginary part of the hth Fourier coefficient of the tangential relative displacement are computed in a similar way. With these partial derivatives the tangent stiffness matrix of the considered contact element can be built up. This tangent stiffness matrix is then used to assemble the Jacobian matrix needed in the calculation of the nonlinear forced vibrations.

2.5 Resulting Mechanical Model and Solution Procedure. After imposing the cyclic symmetry constraints on the segment interface DOF and on the nonlinear contact forces at the left and at the right shroud contact, the resulting nonlinear system of equations given by Eqs. (16) and (17) can be solved for the unknown harmonic coefficients of the displacement ${}^{(j)}\hat{\mathbf{u}}^{(n)}$, $n=0(1)n_h$. Since only the nonlinear DOF are affected by the nonlinear contact forces, a model reduction to these nonlinear DOF is necessary to limit the number of unknowns in the nonlinear analysis. Two different techniques were used in the analysis. First, the structural matrices of the isolated segment model can be extracted from the finite element code in an already reduced form using the Craig–Bampton method, for example. After imposing the cyclic symmetry constraints to the linear part of the system, the technique presented in Ref. [28] can be used to reduce the number of DOF of the remaining left segment interface DOF. A further exact reduction can be performed by using a dynamic condensation as formulated in Ref. [10] for each harmonic n with $n=0(1)n_h$. An alternative to this combined Craig–Bampton, Tran, and dynamic condensation is the use of the dynamic compliance matrix build up based on normal mode shapes as presented in Ref. [14]. A criterion to chose the required complex mode shapes of the cyclic system for the assembly of the dynamic compliance matrix is also given in Ref. [14]. Again, only the part of the nonlinear DOF is required resulting in a compact model suitable for the nonlinear forced response analysis.

Since the resulting system has to be solved with a nonlinear solver, the resulting nonlinear system of equations has to be reformulated in a real form, that is

$${}^{(j)}\hat{\mathbf{u}}^{(n)} = \left[\Re\{{}^{(j)}\hat{\mathbf{u}}^{(n)}\}^T \quad \Im\{{}^{(j)}\hat{\mathbf{u}}^{(n)}\}^T\right]^T \tag{39}$$

with similar expressions for the nonlinear contact forces, for the excitation forces and for the dynamic stiffness matrix and the dynamic compliance matrix, respectively, see also Petrov [12], for example. The system of the nonlinear equations is solved using an implementation of the hybrid Powell algorithm in combination with a predictor-corrector continuation method [29]. The hybrid Powell algorithm is able to approximate the needed Jacobian matrix based on finite differences. The finite difference approxima-

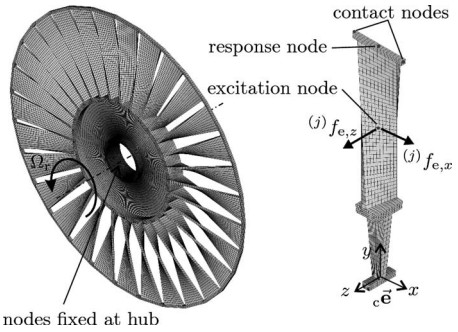

Fig. 6 Model of a shrouded turbine blading

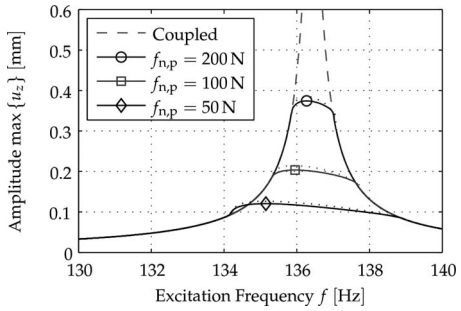

Fig. 8 Response for different values of the normal preload (spatial periodicity $m=1$)

tion of the Jacobian matrix is very cost-intensive, therefore a great gain in terms of the computational efficiency is now obtained by using the procedure presented in the previous section for the direct calculation of the Jacobian matrix. In the predictor-step of the solution procedure, a prediction of the next solution is made based on a tangent or a secant predictor. In a subsequent correction step, the prediction is corrected by the nonlinear solver. In this correction step, an augmented system of nonlinear equations is solved using the hybrid Powell algorithm in order to include the excitation frequency as an unknown into the analysis as it is required for the continuation method, see Seydel [29]. It should be remarked that the presented method is not limited to superharmonics only. By an appropriate choice of the fundamental harmonic in terms of the spatial periodicity m, subharmonics can directly be included in the forced response analysis without any modification of the computational procedure [30].

3 Numerical Example—Analysis of a Shrouded Blading

The presented dynamic model is exemplified by the analysis of the dynamics of a simplified bladed disk coupled by shroud contacts shown in Fig. 6. The model was created in the commercial finite element code ANSYS and consists of 3579 four-node hexahedral elements with 5224 nodes. The material properties were chosen to be according to standard values of steel. The corresponding nodal diameter map of the analyzed system is given in Fig. 7. This model shows essentially the same dynamic properties as a real shrouded bladed disk. In this example, one node placed in the middle of the airfoil is excited by a single force ($^{(j)}f_{e,x} = {}^{(j)}f_{e,z} = 1/\sqrt{2}N$). It is remarked that the presented model is also capable of using a distributed pressure field as an excitation source. The vibration response in the z-direction of a node place at the middle of the tip shroud is shown in the following graphs. The vibration response is defined as $\max\{u_z(l)\}$ for $l=0(1)N-1$, that is the maximum of the magnitude of the time signal obtained from the inverse FFT. The coefficients used in Rayleigh's damping hypothesis for the viscous damping matrix are chosen to be $\alpha = 2.5\ \mathrm{s}^{-1}$ and $\beta = 1.0\times10^{-7}$ s. The forced response of the first vibration family for different numbers of contact node pairs was virtually identical, therefore only one matching contact node pair was used in this case to apply the three-dimensional contact element. For higher vibration modes this can be different and a higher degree of discretization will be necessary. This can easily be achieved by increasing the number of contact node pairs at the cost of a higher computational effort.

In the first example, the calculation of the forced response under consideration of friction damping effects is done. To this end, a monofrequent excitation with a spatial periodicity of $m=1$ has been selected in order to compare the results for different number of harmonics n_h. This corresponds in this case directly to an engine order type excitation with $EO=1$ and excites mainly the first family mode shape of one nodal diameter (backward traveling wave). In Fig. 8, the forced response is shown for different normal preloads $f_{n,p}$. As the normal load decreases, the maximum response also deceases as the friction damping effects increase. The responses shown in Fig. 8 are computed by using $n_h=1$ (dotted lines) and $n_h=3$ harmonics (solid lines). As it can be seen, the analysis performed with a monofrequent approximation (zero and first order terms) leads to an overestimation of the response compared with the result computed with three harmonics (zero, first, second, and third order terms). In addition, the response computed for a fully stuck contact is also shown in this figure. The question arises how many harmonics have to be kept in the analysis in order to obtain converging results. A convergence study revealed that an approximation using three harmonics gives good results with a satisfactory computational effort compared with higher order approximations. In Fig. 9, results are shown again for an excitation with $m=1$ and a static preload of $f_{n,p}=50$ N. The response computed with just one harmonic ($n_h=1$) overestimates in this case the response. Increasing the number of harmonics to more than three results only in minor modifications of the response.

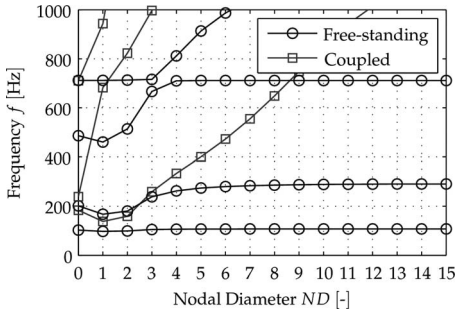

Fig. 7 Nodal diameter map of the analyzed shrouded turbine blading

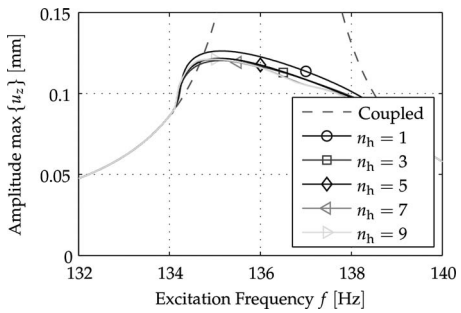

Fig. 9 Response for a different number of harmonics (spatial periodicity $m=1$, normal preload $f_{n,p}=50$ N)

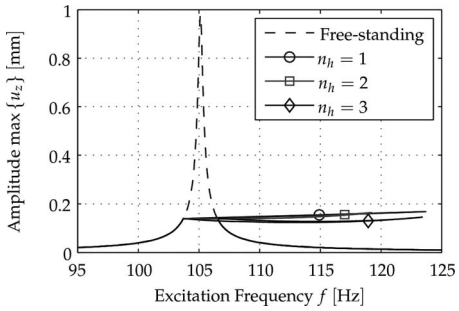

Fig. 10 Response for a different number of harmonics (spatial periodicity m=3, initial gap g=0.1 mm)

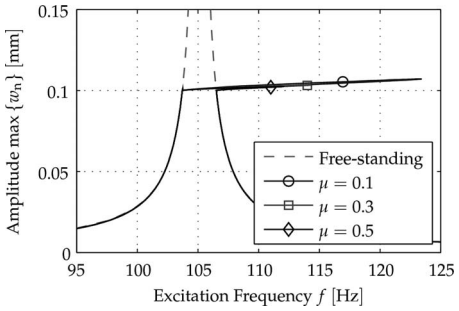

Fig. 12 Relative displacement response for different values of the coefficient of friction (spatial periodicity m=3, gap g =0.1 mm)

In the second example, the response of the shrouded blading is computed by considering the effect of an initial gap on the dynamics of the system. It is assumed that an initial gap of g =0.1 mm exists between the two shroud contact interfaces. A spatial periodicity of m=3 is assumed in this analysis. Again, the excitation is modeled as monofrequent and, therefore, corresponds to an engine order type excitation with EO=3. In Fig. 10, the response is shown for different number of harmonics. The strong nonlinear stiffening effect of the elastic impact on the vibration response can be clearly seen in this graph. If the amplitude of the response is low, the shroud interfaces do not get in contact and the system behavior is linear. As soon as the amplitude levels reach a limit given by the gap g between the shroud contact interfaces, elastic impacts occur resulting in strong stiffening effects. The corresponding relative displacement amplitude in the normal direction of the shroud contact is shown in Fig. 11. The effect of the initial gap (g=0.1 mm) on the relative displacement response is clearly visible. It should be noted that during the elastic impacts also a tangential sliding occurs in the contact leading to an energy dissipation. Therefore, the coefficient of friction has also a strong impact on the response of a system with an initial gap, see Fig. 12. The other important contact parameter in the analysis of a system with an initial gap is the contact stiffness. A high value of the contact stiffness is necessary to represent the dynamics of the system with sufficient accuracy. Unfortunately, a high contact stiffness value can lead to numerical problems in the points of the frequency response where the system changes its behavior from linear to nonlinear and vice versa. A study of the effect of the contact stiffness is shown in Fig. 13 for an approximation of the response using three harmonics. Increasing the value of the contact stiffness leads to a strong increase in the stiffening effect caused by the elastic impacts accompanied by a reduction in the maximum response. Converged results in terms of the resonance frequencies for the fully coupled case have been obtained for a contact stiffness of $k_i = 1.0 \times 10^7$ N/m, $i = x, y, z$, by using a method presented in Ref. [8].

4 Summary and Outlook

In this paper, a MHBM has been derived in detail for the calculation of the nonlinear forced response of cyclic symmetric bladed disk models. The description of the bladed disk is based on three-dimensional finite element models. In order to describe the contact forces with sufficient accuracy, a state-of-the-art three-dimensional contact model capable of representing the possible stick-slip-separation contact states has been applied. The resulting periodic contact forces are computed in the time domain and transformed into the frequency domain using the FFT according to the AFT/HFT procedure. This approach was chosen because of its high flexibility to include also other friction characteristics than the Coulomb friction law. The chosen AFT/HFT approach leads to a very fast computation of the resulting frequency domain representation of the nonlinear contact forces due to the high efficiency of the FFT algorithm. Furthermore, a formulation for the tangent stiffness matrix of the three-dimensional contact model consistent with the AFT/HFT formulation and the FFT has been given for the first time. The use of this tangent stiffness matrix to build up the Jacobian matrix needed in the nonlinear solution procedure leads to great advantage in terms of computational efficiency compared with previously used finite difference computations of the Jacobian matrix. The resulting system of nonlinear equations is solved using a predictor-corrector continuation method. It should be noted that also the zero order term, that is the static term, is included within this MHBM analysis. The presented mechanical model has been implemented in a numerical code and is exemplified by analyzing the nonlinear dynamics of a turbine blading coupled by shrouds. The friction damping effect as well as the effect of an initial gap on the system's response has been shown. In a further work, this code will be used for extensive numerical studies of shrouded blading dynamics. Furthermore, the capability of the code will be extended in terms of a stability analysis using Hill's or Floquet's theory.

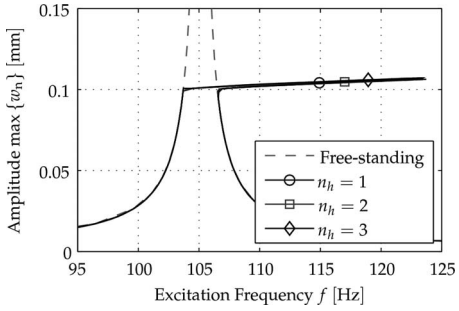

Fig. 11 Relative displacement response in normal direction for a different number of harmonics (spatial periodicity m=3, gap g=0.1 mm)

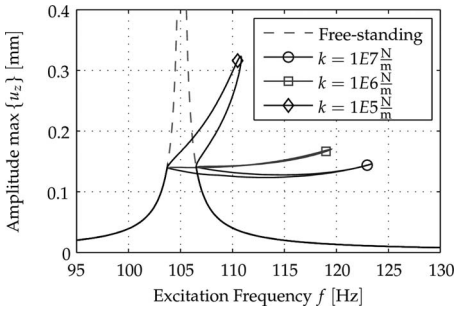

Fig. 13 Response for different values of the contact stiffness (spatial periodicity m=3, gap g=0.1 mm)

Acknowledgment

The work described in this paper has been carried out within the national research project *Höher Harmonische Balance* funded by the Deutsche Forschungsgemeinschaft (DFG) and the Forschungsvereinigung Verbrennungskraftmaschinen e.V. (FVV).

References

[1] Yang, B. D., and Menq, C. H., 1996, "Modeling of Friction Contact and Its Application to the Design of Shroud Contact," ASME Paper No. 96-GT-472.
[2] Yang, B. D., Chen, J. J., and Menq, C. H., 1998, "Prediction of Resonant Response of Shrouded Blades With Three-Dimensional Shroud Constraint," ASME Paper No. 98-GT-485.
[3] Chen, J. J., and Menq, C. H., 1998, "Prediction of Resonant Response of Frictionally Constrained Blade Systems Using Constrained Mode Shapes," ASME Paper No. 98-GT-548.
[4] Sextro, W., 2000, "The Calculation of the Forced Response of Shrouded Blades With Friction Contacts and Its Experimental Verification," ASME Paper No. 2000-GT-540.
[5] Sextro, W., 2007, *Dynamical Contact Problems With Friction—Models, Methods, Experiments and Applications*, 2nd ed., Springer, Berlin, Germany.
[6] Panning, L., Popp, K., Sextro, W., Götting, F., Kayser, A., and Wolter, I., 2004, "Asymmetrical Underplatform Dampers in Gas Turbines Bladings: Theory and Application," ASME Paper No. GT2004-53316.
[7] Szwedowicz, J., Sextro, W., Visser, R., and Masserey, P. A., 2003, "On Forced Vibration of Shrouded Turbine Blades, ASME Paper No. GT2005-69062.
[8] Szwedowicz, J., Slowik, S., Mahler, A., and Hulme, C. J., 2005, "Nonlinear Dynamic Analysis of a Gas Turbine Blade for Attainment of Reliable Shroud Coupling," ASME Paper No. GT2005-69062.
[9] Siewert, C., Panning, L., Gerber, C., Masserey, P. A., 2008, "Numerical and Experimental Damping Prediction of a Nonlinearly Coupled Low Pressure Steam Turbine Blading," ASME Paper No. GT2008-51073.
[10] Poudou, O., and Pierre, C., 2003, "Hybrid Frequency-Time Domain Methods for the Analysis of Complex Structural Systems With Friction Damping," Collection of Technical Papers—AIAA/ASME/ASCE/AHS/ASC Structural Dynamics and Materials Conference, Norfolk, VA, Vol. 1, pp. 111–124.
[11] Chen, J. J., and Menq, C. H., 1999, "Prediction of Periodic Response of Blades Having 3D Shroud Constraints," ASME Paper No. 99-GT-289.
[12] Petrov, E. P., 2004, "A Method for Use of Cyclic Symmetry Properties in Analysis of Nonlinear Multiharmonic Vibrations of Bladed Disks," ASME J. Turbomach., **126**, pp. 175–183.
[13] Laxalde, D., Thouverez, F., Sinou, J. J., and Lombard, J. P., 2006, "Forced Response Analysis of Blisks With Friction Ring Dampers," *Proceedings of 7th IFToMM International Conference on Rotor Dynamics 2006*, Vienna, Austria.
[14] Siewert, C., Krack, M., Panning, L., and Wallaschek, J., 2008, "The Nonlinear Analysis of the Multiharmonic Forced Response of Coupled Turbine Blading," *Proceedings of the 12th International Symposium on Transport Phenomena and Dynamics of Rotating Machinery 2008*, Honolulu, HI.
[15] Cook, R. D., Malkus, D. S., Plesha, M. E., and Witt, R. J., 2002, *Concepts and Applications of Finite Element Analysis*, 4th ed., Wiley, New York.
[16] Gasch, R., and Knothe, K., 1989, *Strukturdynamik Bd. 2—Kontinua und Ihre Diskretisierung*, 1st ed., Springer, Berlin, Germany.
[17] Thomas, D. L., 1979, "Dynamics of Rotationally Periodic Structures," Int. J. Numer. Methods Eng., **14**, pp. 81–102.
[18] Yang, B. D., Chu, M. L., and Menq, C. H., 1998, "Stick-Slip-Separation Analysis and Non-Linear Stiffness and Damping Characterization of Friction Contacts Having Variable Normal Load," J. Sound Vib., **210**(4), pp. 461–481.
[19] Petrov, E. P., and Ewins, D. J., 2002, "Analytical Formulation of Friction Interface Elements for Analysis on Nonlinear Multi-Harmonic Vibrations of Bladed Discs Discs," ASME Paper No. GT-2002-30325.
[20] Cigeroglu, E., and Menq, C. H., 2007, "Wedge Damper Modeling and Forced Response Prediction of Frictionally Constrained Blades," ASME Paper No. GT2007-27963.
[21] Cigeroglu, E., An, N., and Menq, C. H., 2007, "A Microslip Friction Model With Normal Load Variation Induced by Normal Motion," Nonlinear Dyn., **50**(3), pp. 609–626.
[22] Petrov, E. P., 2007, "Explicit Finite Element Models of Friction Dampers in Forced Response Analysis of Bladed Discs," ASME No. Paper GT2007-27980.
[23] Cigeroglu, E., and Menq, C. H., 2008, "A Microslip Friction Model for the Analysis of Frictionally Damped Turbine Blades," *Proceedings of the 9th International Conference on Vibrations in Rotating Machinery 2008*, Exceter, UK.
[24] Cameron, T. M., and Griffin, J. H., 1989, "An Alternating Frequency/Time Domain Method for Calculating the Steady-State Response of Nonlinear Systems," ASME J. Appl. Mech., **56**, pp. 149–154.
[25] Newland, D. E., 2005, *An Introduction to Random Vibrations, Spectral and Wavelet Analysis*, 3rd ed., Dover, New York.
[26] Ling, F. H., and Wu, X. X., 1987, "Multi-Harmonic Analysis of Dry Friction Damped Systems Using an Incremental Harmonic Balance Method," Int. J. Non-Linear Mech., **22**(2), pp. 89–98.
[27] Cardona, A., Lerusse, A., and Géradin, M., 1998, "Fast Fourier Nonlinear Vibration Analysis," Comput. Mech., **22**, pp. 128–142.
[28] Tran, D. M., 2001, "Component Mode Synthesis Methods Using Interface Modes. Application to Structures With Cyclic Symmetry," Comput. Struc., **79**(2), pp. 209–222.
[29] Seydel, R., 1994, *Practical Bifurcation and Stability Analysis—From Equilibrium to Chaos*, 2nd ed., Springer, Berlin, Germany.
[30] Petrov, E. P., 2006, "Direct Parametric Analysis of Resonance Regines for Nonlinear Vibrations of Bladed Discs," ASME Paper No. GT2006-90147.